Rotationally resolved photoionization dynamics of hot CO fragmented from OCS

Anouk M. Rijs, Ellen H. G. Backus, Cornelis A. de Lange, Maurice H. M. Janssen, Nicholas P. C. Westwood, Kwanghsi Wang, and Vincent McKoy

Citation: The Journal of Chemical Physics **116**, 2776 (2002); doi: 10.1063/1.1434993
View online: http://dx.doi.org/10.1063/1.1434993
View Table of Contents: http://scitation.aip.org/content/aip/journal/jcp/116/7?ver=pdfcov
Published by the AIP Publishing

Rotationally resolved photoionization dynamics of hot CO fragmented from OCS

Anouk M. Rijs
Laboratory for Physical Chemistry, University of Amsterdam, Nieuwe Achtergracht 127-129, 1018 WS Amsterdam, the Netherlands, and Laser Centre and Department of Chemistry, Vrije Universiteit, De Boelelaan 1083, 1081 HV Amsterdam, the Netherlands

Ellen H. G. Backus
Laboratory for Physical Chemistry, University of Amsterdam, Nieuwe Achtergracht 127-129, 1018 WS Amsterdam, the Netherlands

Cornelis A. de Lange
Laboratory for Physical Chemistry, University of Amsterdam, Nieuwe Achtergracht 127-129, 1018 WS Amsterdam, the Netherlands, and Department of Chemistry, The University, Southampton SO17 1BJ, United Kingdom

Maurice H. M. Janssen
Laser Centre and Department of Chemistry, Vrije Universiteit, DeBoelelaan 1083, HV Amsterdam, the Netherlands

Nicholas P. C. Westwood
Guelph-Waterloo Centre for Graduate Work in Chemistry, Department of Chemistry and Biochemistry, University of Guelph, Guelph, Ontario, N1G 2W1, Canada

Kwanghsi Wang and Vincent McKoy
Arthur Amos Noyes Laboratory for Chemical Physics, California Institute of Technology, Pasadena, California 91125

(Received 2 April 2001; accepted 21 November 2001)

The photoionization dynamics of rotationally hot CO, photodissociated from OCS, have been studied using laser photoelectron spectroscopy via the intermediate $B\,^1\Sigma^+$ Rydberg state leading to the $X\,^2\Sigma^+$ of the ion. The photodissociation of OCS near 230 nm produces rotationally hot, but vibrationally cold CO ($X\,^1\Sigma^+, N'', v''=0,1$) fragments along with S (^1D) atoms. These high rotational levels show photoelectron spectra with a very strong $\Delta N=0$ transition and weaker $\Delta N=\pm 1$, ± 2, and ± 3 transitions. Agreement between measured and calculated spectra is good and suggests that there is significant angular momentum coupling in the photoelectron orbital. In the ionization step not only $\Delta v=0$, but also off-diagonal, non-Franck–Condon ($\Delta v\neq 0$) transitions are observed. The intensities of these transitions vary strongly within the region studied and can be explained by the excitation of superexcited Rydberg states with an $A\,^2\Pi$ core. © *2002 American Institute of Physics.* [DOI: 10.1063/1.1434993]

I. INTRODUCTION

OCS belongs to the linear triatomic 16 valence electron systems such as CO_2, CS_2, and N_2O. Like all these 16 valence electron systems, OCS is linear ($C_{\infty v}$) in the ground state, and either linear or bent in the excited states. Electronic transitions from the ground state ($\tilde{X}\,^1\Sigma^+$) to $^1\Sigma^-$ and $^1\Delta$ excited states are forbidden in the linear geometry due to the selection rules. However, these transitions are weakly allowed in the bent configuration (C_s). At around 230 nm two dissociation pathways of OCS can be followed via the $^1\Delta$ and the $^1\Sigma^-$ excited states ($C_{\infty v}$), which correspond to the $2\,^1A'$, $2\,^1A''(^1\Delta)$, and $1\,^1A''(^1\Sigma^-)$ states in the bent geometry (C_s).[1] The photodissociation of OCS near 230 nm occurs mainly via the $2\,^1A'$ state producing rotationally hot, but vibrationally cold CO ($X\,^1\Sigma^+$) fragments along with S (^1D) atoms. As the fragments separate, a strong torque is exerted on the CO fragments, leading to rotationally hot CO. Several photodissociation studies of OCS have been carried out by probing the photofragment product channels, either by laser-induced fluorescence,[2,3] by ion imaging combined with $(2+1)$ REMPI,[4–7] or by REMPI in combination with photoelectron spectroscopy.[8–10] The CO rotational distribution shows a bimodal structure,[2–5,8–10] with maxima at $N''=50$ and $N''=63$. This bimodal distribution is mainly due to two different processes on the $2\,^1A'$ ($^1\Delta$) surface, namely direct dissociation and surface crossing to the ground state.[5]

Resonance enhanced multiphoton ionization in combination with kinetic energy resolved photoelectron spectroscopy (REMPI-PES) is the method of choice to obtain detailed information about the spectroscopy and the photoionization dynamics of the intermediate state. With a ''magnetic bottle'' high-resolution electron spectrometer, rotationally resolved photoelectron spectra and ion rotational branching ratios can be obtained. These rotationally resolved photoelectron spectra provide information on the photoionization dynamics and on the exchange of angular momentum between the ion and

the leaving photoelectron. To obtain rotationally resolved photoelectron spectra, molecules with sizable rotational constants are very suitable, providing ionic rotational spacings that are large compared to the resolution of the electron spectrometer. A well-studied class of molecules with large rotational constants are the diatomic hydride radicals such as OH,[11] NH,[12,13] and SH.[14,15]

In this work, rotationally resolved photoelectron spectroscopy is carried out on hot CO photofragments produced in the photodissociation of OCS. The rotational constant of CO^+ in the $X\,^2\Sigma^+$ ionic ground state is only 1.9677 cm^{-1}.[16] Nevertheless, the high rotational excitation of the CO fragment in the present experiment leads to large ionic spacings, and thus allows the measurement of photoelectron kinetic energies with rotational resolution. Rotationally resolved laser photoelectron spectroscopy was recently applied to the comparable isoelectronic N_2 photofragments produced in the photodissociation of N_2O at ~203 nm.[17] By combining our PES results with the results of *ab initio* quantum-chemical calculations,[18,19] detailed information was obtained on the dynamics of the photoionization process.

In this work the rotationally resolved laser photoelectron spectroscopy of hot CO fragments is studied via a two-step ionization process using the $B\,^1\Sigma^+$ $3s\sigma$ (6σ) Rydberg state as a stepping-stone. The intermediate $B\,^1\Sigma^+$ Rydberg state represents the lowest member of a Rydberg series converging upon the $X\,^2\Sigma^+$ ionic ground state of CO^+, and is located ~10.7 eV above the electronic ground state of CO ($X\,^1\Sigma^+$). Several groups have measured CO produced in the photodissociation of OCS using $(2+1)$ REMPI via the $B\,^1\Sigma^+$ Rydberg state in the wavelength range near 230 nm.[4–10] The $B-X$ transition in CO has also been studied employing high-resolution vacuum ultraviolet (VUV) emission and absorption spectroscopy. Accurate vibrational and rotational constants of the $B\,^1\Sigma^+$ state, based on the observation of rotational levels $N'=0-63$ (R branch) and $N'=0-33$ (P branch), were obtained.[20]

The one-photon ionization step from the intermediate $B\,^1\Sigma^+$ Rydberg state to the $X\,^2\Sigma^+$ ionic ground state of CO^+ is expected to be highly Franck–Condon allowed, implying a strong $\Delta v=0$ propensity. However, in a previous (REMPI-PES) study of CO via the $B\,^1\Sigma^+$ Rydberg state Sha *et al.*[21] observed significant non-Franck–Condon behavior in the photoionization process. This is very surprising given the strong similarity between the intermediate ($R_e=1.1197$ Å[20]) and the ionic ground state ($X\,^2\Sigma^+$, $R_e=1.1151$ Å[22]) and the small difference in vibrational spacings of CO ($B\,^1\Sigma^+$) and CO^+ ($X\,^2\Sigma^+$). A Rydberg–valence interaction of the $B\,^1\Sigma^+$ Rydberg state, which can cause the non-Franck–Condon transitions in the photoelectron spectra, does not seem to be operational.[21] For the B state, neither indications for predissociation nor perturbations arising from closely neighboring electronic states have been observed.[23] Sha *et al.*[21] reported a connection between the non-Franck–Condon behavior and the observed angular distribution of the photoelectrons, but the essence of the mechanism responsible for the non-Franck–Condon behavior in the photoionization step remains in the dark. We have explored this non-diagonal behavior in more detail, and we shall present a very likely explanation, namely the excitation of appropriate ''superexcited'' states in the $X\,^2\Sigma^+$ ionization continuum.

A brief description of the experimental setup is given in Sec. II, while the theoretical formulation employed is outlined in Sec. III. The experimental results and a discussion and comparison with the *ab initio* quantum-chemical calculations are presented in Sec. IV. In Sec. V the conclusions are summarized.

II. EXPERIMENT

The experimental setup has been described in great detail previously.[10] Therefore, we shall give only a brief description here.

The laser system consists of a XeCl excimer laser (Lumonics HyperEx 460) producing pulsed radiation with a fixed wavelength of 308 nm and a pulse duration of ~10 ns. The light pulses are generated with a repetition rate of 30 Hz and have an energy of 200 mJ/pulse. The output of the excimer laser is used to pump a Lumonics HyperDye 500 dye laser (bandwidth 0.08 cm^{-1}), operating on Coumarine 460. The dye laser output (about 460 nm) is frequency doubled in a Lumonics HyperTrack 1000 using a BBO crystal resulting in 10 ns pulses with a maximum energy of about 15 mJ and a bandwidth of ~0.2 cm^{-1}. During the wavelength scans the power of the 230 nm laser beam is monitored with a photodiode. The laser light is focused into the ionization region of a ''magnetic bottle'' spectrometer by a quartz lens with a focal length of 25 mm. In the present experiments, both wavelength scans and photoelectron spectra are obtained by using the ''magnetic bottle'' spectrometer in the electron detection mode. In this case, the spectrometer operates with a collection efficiency of ~50% and an energy resolution of about 10 meV.

The rotationally hot CO photofragments are generated *in situ* by one-photon dissociation of OCS (Matheson). The OCS gas sample is effusively introduced into the ionization chamber of the ''magnetic bottle'' spectrometer. The photodissociation of OCS and the subsequent $(2+1)$ REMPI of the rotationally excited CO fragments are performed with the same laser photons of 230 nm. For wavelength and photoelectron kinetic energy calibration well-known resonances of xenon atoms at a two-photon energy of 88 379.6 cm^{-1} [24] and of sulfur atoms at a two-photon energy of 86 921.4 cm^{-1} [25] are used.

III. THEORETICAL FORMULATION

The general theory of molecular REMPI processes used in the present study has been described previously.[19] Here we present just a brief outline of some essential features as it is used to obtain rotationally resolved photoelectron spectra. In the present case, ionization originating from each of the $(2J+1)$ magnetic sublevels of the $B\,^1\Sigma^+$ state of CO forms an independent channel. The total cross section σ for ionization of a J level of the intermediate state leading to a J^+ level of the ion can be written as

$$\sigma \propto \sum_{\substack{lm \\ M_J M_{J^+}}} \rho_{M_J M_{J^+}} |C_{lm}(M_J M_{J^+})|^2, \tag{1}$$

where $\rho_{M_J M_{J^+}}$ is the population of a specific M_J level of the intermediate state. The coefficients $C_{lm}(M_J M_{J^+})$ of Eq. (1) are related to the probability for photoionization of the M_J level of the intermediate state leading to the M_{J^+} level of the ionic state. For a Hund's case (b) coupling scheme, the $C_{lm}(M_J M_{J^+})$ coefficients have the form

$$C_{lm}(M_J,M_{J^+})=\sqrt{\frac{4\pi}{3}}[(2N^+ +1)(2N+1)(2J+1)(2J^+ +1)(2S+1)]^{1/2}\sum\ (-1)^P(2N_t+1)\begin{pmatrix} N & S & J \\ M & M_s & -M_J\end{pmatrix}$$
$$\times\begin{pmatrix} N^+ & S^+ & J^+ \\ M^+ & M_{s^+} & -M_{J^+}\end{pmatrix}\begin{pmatrix} S^+ & 1/2 & S \\ M_{s^+} & M_\sigma & -M_s\end{pmatrix}\begin{pmatrix} N^+ & N & N_t \\ -M^+ & M & m_t\end{pmatrix}\begin{pmatrix} N_t & 1 & l \\ -m_t & \mu_0 & -m\end{pmatrix}$$
$$\times\sum_{\substack{\mu\\ \lambda_t}}\ (-1)^{-\Lambda^+-\mu}\tilde{I}_{l\lambda\mu}\begin{pmatrix} N^+ & N & N_t \\ -\Lambda^+ & \Lambda & \lambda_t\end{pmatrix}\begin{pmatrix} N_t & 1 & l \\ -\lambda_t & \mu & -\lambda\end{pmatrix}, \tag{2}$$

with

$$P=M^+ +M_{J^+}-M+\mu_0-N-N^+ +S+\tfrac{1}{2}, \tag{3}$$

where λ and m are projections of the photoelectron's angular momentum l in the molecular and laboratory frames, respectively, N is the electronic plus rotational angular momentum of the intermediate state, N_t is the angular momentum transfer, Λ is the projection of electronic orbital angular momentum along the internuclear axis, S is the total spin. $\tilde{I}_{l\lambda\mu}$ is the vibrationally averaged photoelectron matrix element between the resonant state and the photoelectron continuum wavefunction, and μ and μ_0 are the light polarization indices in the molecular and laboratory frames, respectively. The symbols with superscript + are related to these same quantities in the ion. Equation (2) provides a selection rule of the form

$$\Delta N+l=odd, \tag{4}$$

for photoionization. Since the $3s\sigma$ (6σ) orbital has strong s character ($\sim$74% s, 24% p, and 2% d at $R_e=2.1322a_0$), the p-wave component of the photoelectron matrix element is expected to be dominant with some weaker contributions from even partial waves. Both even and odd ΔN transitions are hence expected.

For the wave function of the $B\,^1\Sigma^+$ resonant state, we use the improved virtual orbital (IVO) method[26] in which the core orbitals are taken to be those of the fully relaxed $X\,^2\Sigma^+$ ion and the 6σ resonant orbital is obtained as an eigenfunction of the static-exchange potential of the core. The orbital basis functions used in these calculations are the same as in Ref. 27. With this basis and choice of wave functions, we obtain a selfconsistent-field energy of 108.605 407 a.u. at $R_e=2.1322a_0$ for the $B\,^1\Sigma^+$ state.

For the final state we assume a frozen-core Hartree–Fock model in which the core orbitals are taken to be those of the $^2\Sigma^+$ ion and the photoelectron orbital is a solution of the one-electron Schrödinger equation. To obtain the photoelectron orbitals, we used an iterative procedure, based on the Schwinger variational principle,[18] to solve the Lippmann–Schwinger equation associated with the one-electron Schrödinger equation.

IV. RESULTS AND DISCUSSION

The photodissociation of OCS at 230 nm produces rotationally excited CO in the electronic ground state, mainly in its vibrational ground state, but also in the first vibrationally excited state. Figure 1 presents the excitation spectrum of CO photofragments in the two-photon energy range 86 850–87 100 cm^{-1}. CO is photoionized in a two-step process, starting from the $X\,^1\Sigma^+$ $(v''=0,1;N'')$ ground state via the $B\,^1\Sigma^+$ $(v'=0,1;N')$ intermediate Rydberg state to the $X\,^2\Sigma^+$ $(v^+=0,1;N^+)$ lowest ionic state. The spectra were obtained by monitoring photoelectrons with a kinetic energy of about 2.15 eV. This excitation scan shows a well-resolved bimodal distribution of the Q branch of CO, extending from $N'=37$ up to $N'=87$ with two maxima at $N'=50$ and $N'=63$. At $\sim$86 917 cm^{-1} CO in low rotational states near the origin is detected. At lower energies, the first hot band $(v'=1;N'\leftarrow v''=1;N'')$ is observed, also with a bimodal rotational distribution, and at 86 856 cm^{-1} the origin of this hot band is located. Simultaneously, in another kinetic energy window at about 1.6 eV, ionization of $S(^1D_2)$ atoms via the $S\,((^2D^o)7f)$ states is observed. These resonances are used

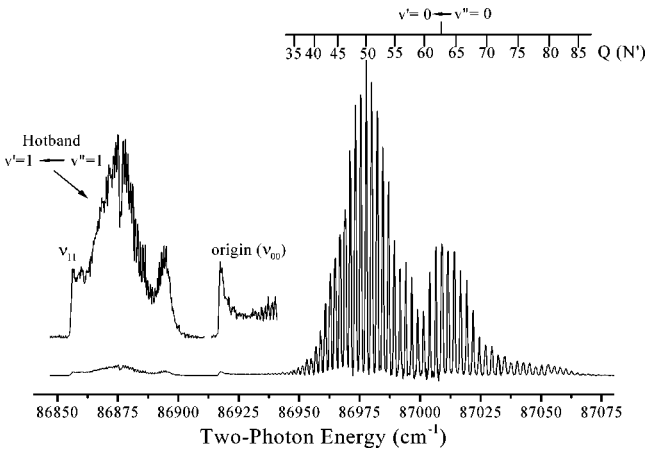

FIG. 1. Rotationally resolved (2+1) REMPI excitation spectrum with electron detection of the Q branch of the $B\,^1\Sigma^+\leftarrow\leftarrow X\,^1\Sigma^+$ transition of rotationally hot CO $(v'=0,1;N')$ photofragments in the energy window 86 840–87 075 cm^{-1} (vacuum energies).

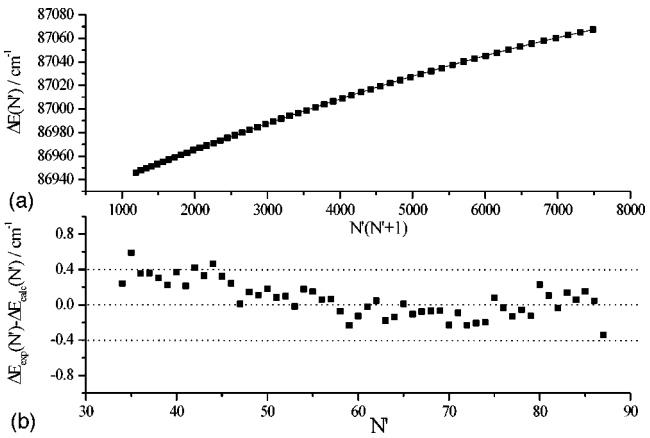

FIG. 2. (a) Rotational fit of the measured line positions for the $B\,^1\Sigma^+$ $(v'=0) \leftarrow\leftarrow X\,^1\Sigma^+$ $(v''=0)$ transition in CO, based on the known rotational constants of the vibrationless ground state $X\,^1\Sigma^+$ $(v''=0)$ (Ref. 28) and the first-order rotational constant of the B state (Ref. 20). Results are given in Table I. (b) Residual plot, the difference between experimental and calculated line positions.

for wavelength calibration. In addition to our earlier results,[10] the much weaker O and S branches are observed around 86 500–86 650 cm^{-1} and 87 250–87 550 cm^{-1}, respectively. These O and S branches show also a bimodal distribution, with maxima occurring at the same rotational levels $N'=50$ and 63 as in the Q branch (not shown).

The assignment of the spectra of Fig. 1 and the rotational fit of the Q branch were performed in an iterative fashion. The $B\,^1\Sigma^+$ excited state rotational constants were determined by fitting all the rotational energies of the Q branch to the following expression:

$$\Delta E(N') = \nu_{00} + (B_0' - B_0'')N'(N'+1) - (D_0' - D_0'')N'^2(N'+1)^2 + (H_0' - H_0'')N'^3(N'+1)^3. \quad (5)$$

In our excitation spectrum of rotationally excited CO, we measured only high rotational levels from $N'=34$ up to $N'=87$. These high rotational levels mainly determine the higher-order rotational constants D_0 and H_0. On the other hand, the first-order rotational constant B_0 predominantly depends on the position of low rotational levels. In order to perform the best rotational analysis possible, we use the very accurate rotational constant B_0' for the $B\,^1\Sigma^+$ $(v'=0)$ Rydberg state, as well as the value for v_{00}, of Eidelsberg *et al.* [20] With our rotational fit we improve the D_0' and H_0' rotational constants of the CO $B\,^1\Sigma^+$ $(v'=0)$ state. These excited state rotational constants are obtained by using the well-known rotational constants (B_0'', D_0'', and H_0'') of the CO $(X\,^1\Sigma^+)$ ground state.[28] Because of the high rotational excitation observed in the present study, addition of the third-order rotational constant H_0' provides a significant improvement of the rotational fit. The results of this rotational fit are shown in Fig. 2(a), and the difference plot between the experimental and calculated line positions is presented in Fig. 2(b). The improved rotational constants for the CO $B\,^1\Sigma^+$ $(v'=0)$ state are listed in Table I, together with the B_0' and v_{00} values of Eidelsberg *et al.*,[20] and the CO $(X\,^1\Sigma^+)$ ground state

TABLE I. Rotational constants (in cm^{-1}) for the $B\,^1\Sigma^+(v'=0)$ Rydberg state of CO (left column), and a comparison with the literature (Ref. 20) (central column). The ground state rotational constants of CO $X\,^1\Sigma^+$ (Ref. 28) are presented in the right column.

Constants	Present work (cm^{-1})	Ref. values (Ref. 20) (cm^{-1})	$X\,^1\Sigma^+$ constants (Ref. 28)
v_{00}	86 916.18[a]	86 916.18(3)	-
B_0	1.948 186[a]	1.948 186(72)	1.922 629
$D_0 \cdot 10^6$	6.6355(12)	6.784(21)	6.1212
$H_0 \cdot 10^{11}$	−2.161(19)	-	0.5290

[a]Note: fixed at reference values by Eidelsberg *et al.* (Ref. 20), see the center column.

constants.[28] With these improved rotational constants, the O and S branches are recalculated. The residual plots (not shown) are virtually identical to the Q branch plot.

Photoelectron kinetic energy scans were obtained by one-photon ionization from the intermediate CO $B\,^1\Sigma^+$ $(v'=0,1;N')$ state into the continua of the ionic ground state $X\,^2\Sigma^+$ $(v^+=0,1;N^+)$. Because of the high rotational excitation of the CO fragment, the ionic spacings are large enough to measure rotationally resolved photoelectron spectra. Hence, instead of one broad unresolved peak, a rotationally resolved feature is observed. Figure 3 shows the experimental (left) and calculated (right) photoelectron spectra of the vibrationless $Q(66)$ rotational transition at 87 016.7 cm^{-1}. The dominant peak in the experimental photoelectron spectrum at 2.15 eV arises from the $\Delta v=0$ and $\Delta N=N^+-N'=0$ transition. The small neighboring peaks arise from $\Delta N=\pm1$, ±2, or ±3 transitions. These peaks are separated from the main feature by ~32 meV, equivalent to approximately $2B^+N^+$. Here $B^+=1.9677\ cm^{-1}$ (Ref. 16) is the ionic rotational constant, and N^+ signifies the end-over-end rotation.

The rotational structure in the photoelectron spectra of CO is subject to selection rules. For one-photon ionization of the $B\,^1\Sigma^+(v')$ state, the selection rule of Eq. (4), i.e., ΔN

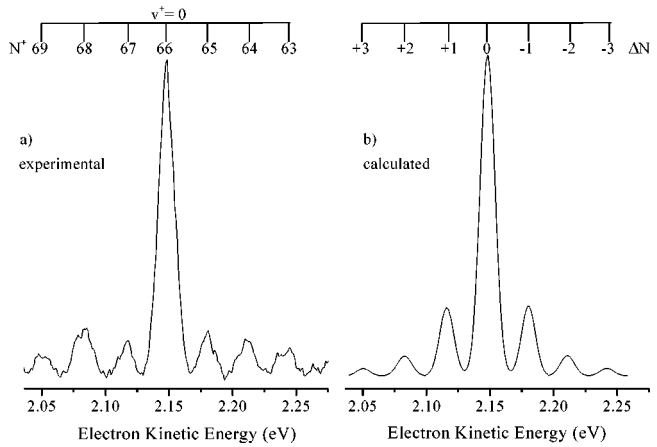

FIG. 3. Experimental (left) and calculated (right) rotationally resolved photoelectron spectra of rotationally hot CO, produced in the photodissociation of OCS. The experimental photoelectron spectrum is obtained by (2+1) photoionization via the $Q(66)$ transition to the intermediate $B\,^1\Sigma^+$ $(v'=0)$ Rydberg state. The calculated spectrum is representative for all photoelectron spectra from $v'=0$ and high N'.

$+l=odd$ applies, where $\Delta N=N^+-N'$ and l is a partial wave component of the photoelectron.[29,30] In the present case the CO Rydberg electron occupies a $3s\sigma$ (6σ) molecular orbital. In an atomic-like picture, ionization of this 6σ ($n=3$) Rydberg electron is expected to lead to p ($l=1$) partial waves, and, on this basis, strong $\Delta N=even$ transitions would be expected. As seen in Fig. 3, in addition to these even $\Delta N=0$, ± 2 peaks, $\Delta N=\pm 1$, ± 3 transitions are also observed. These $\Delta N=odd$ transitions are due to even photoelectron partial waves which, in turn, may arise from p or f components of the $3s\sigma$ orbital in the $B\,^1\Sigma^+$ Rydberg state (an initial-state effect) or from angular momentum coupling in the photoelectron wave function (a final-state effect). Indeed at $R_e=2.1322a_0$, the $3s\sigma$ (6σ) orbital of the $B\,^1\Sigma^+$ state has 74% *s*, 24% *p*, and 2% *d* character. Furthermore, at a kinetic energy of 2.15 eV, the magnitudes of the partial-wave components of the dipole matrix element for ionization out of the $3s\sigma$ orbital are 1.016, 1.568, 1.194, 0.282, and 0.154 (atomic units) for the $l=0$, 1, 2, 3, 4 channels of the σ continuum and 1.245, 0.244, 0.258, and 0.110 for the $l=1$, 2, 3, 4 channels of the π continuum, respectively. The magnitudes of the *s* and *d* wave components of the photoelectron matrix element (1.016 and 1.194, respectively) relative to the *p*-wave component (1.568) in the σ channel are much larger than the ratio of the *p* (24%) to *s* (74%) contributions to the $3s\sigma$ orbital, and a likely explanation is that there is significant angular momentum coupling in the photoelectron orbital. On the other hand, the magnitude of the *d*-wave component (0.244) of the photoelectron matrix element in the π-channel relative to the *p*-wave component (1.24) would be consistent with an initial-state effect arising from the 24% character of the $3s\sigma$ orbital.

The measured (left) and calculated (right) photoelectron spectra of Fig. 3 show the same features: a dominant peak resulting from the $\Delta N=0$ transition, and the neighboring smaller peaks from the $\Delta N=\pm 1$, ± 2, ± 3 transitions. Agreement between the measured and calculated spectra is good in the normal $\Delta v=0$ energy region, but the calculated spectra show stronger $\Delta N=\pm 1$ and weaker $\Delta N=\pm 2$ and ± 3 transitions. Further examination shows a *p*-wave contribution of 99% to the $\Delta N=0$ peak, *s* and *d* wave contributions of 55% and 45%, respectively, to the $\Delta N=1$ peak, and *p* and *f* contributions of 59% and 41%, respectively, to the $\Delta N=2$ peak. It is interesting to note that even though the *s*- and *d*-wave contributions to the photoelectron matrix element in the σ channel are of the same magnitude as that of the *p* wave, the $\Delta N=\pm 1$ transitions are much weaker ($\sim$20%) than that of $\Delta N=0$. To some extent, this may be due to interference in the *d*-wave components of the σ and π channels.

So far we have only considered the rotational structure in our photoelectron kinetic energy measurements. We now focus our attention on the vibrational behavior during the ionization step. Based on the similarity between the $B\,^1\Sigma^+$ Rydberg state and the $X\,^2\Sigma^+$ ionic state potentials, only $\Delta v=0$ transitions would be expected. In order to explore the vibrational branching in the $X\,^2\Sigma^+$ ionic continuum, a two-color ($2+1'$) REMPI-PES experiment would be ideal, because it would allow us to probe the energy in the continuum in a continuous fashion. In our current one-color ($2+1$)

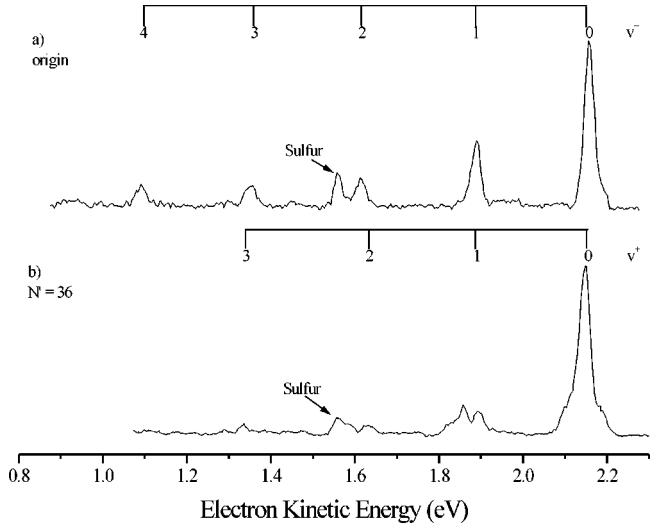

FIG. 4. Photoelectron spectra of CO, resulting from ($2+1$) photoionization via the $B\,^1\Sigma^+$ ($v'=0$) Rydberg state for (a) the origin, and (b) $N'=36$. In both spectra transitions to $X\,^2\Sigma^+$ ($v^+=0,1,2,3,4$) are shown.

REMPI-PES experiment we can employ every populated rotational level associated with the $B\,^1\Sigma^+$ Rydberg state of the rotationally hot CO fragment as a stepping stone. Hence, we can approximate the ($2+1'$) experiment by "tuning" the three-photon energy in the continuum in small steps, determined by the rotational spacing in the *B* state. At every energy thus reached in the continuum, the corresponding PE spectra can be measured. Our results show that for $N'\geqslant 48$ the expected $\Delta v=0$ behavior is indeed observed. However, in the narrow energy region where the three-photon energy lies between 16.16–16.18 eV, strong deviations from the expected $\Delta v=0$ propensity occur. In Fig. 4(a) we show a PE spectrum obtained via rotational levels of the *B* state close to the band head ($N'=0$). At this three-photon energy $\sim$130 376 cm^{-1}, corresponding to 16.16 eV, the strongest deviation from diagonal Frank–Condon behavior, with vibrational excitation up to $v^+=4$ is observed. Figure 4(b) shows similar, although less pronounced, $\Delta v\neq 0$ behavior at a three-photon energy of 130 424.4 cm^{-1}, corresponding to 16.17 eV, where the $B\,^1\Sigma^+$ ($v'=0,N'=36$) level of rotationally excited CO is employed as a stepping stone. Above $\sim$130 460 cm^{-1} ($N'\approx 48$) these nondiagonal transitions are not observed anymore. Clearly, the appearance of these significant non-Frank–Condon transitions depends strongly on the laser wavelength, and takes place in a narrow three-photon energy region of less than 100 cm^{-1} (12 meV) only. A previous REMPI-PES study on CO via the *B* state of Sha *et al.*,[21] taken at a single wavelength in the same energy region, also showed comparably strong non-Franck–Condon behavior. In a sense the significant rotational excitation with which the CO molecules are formed allows us to explore the ionization continua in rather small energy steps. This brings to light variations in vibrational branching ratios that would be hard to observe otherwise.

In our experiments, an energy region of a few eV above the first ionic limit is accessed. It is well known that in laser

photoelectron spectroscopy an abundance of neutral states located above the lowest ionic limit and belonging to Rydberg series converging upon higher ionic limits, often termed superexcited states, can play a key role in photoionization.[15,31,32] More often than not there is a competition between direct ionization and excitation of such superexcited states, which can subsequently undergo a variety of decay processes. These decay processes may include autoionization, (pre)dissociation, or absorption of additional photons. The ground ionic threshold $X\,^2\Sigma^+$ of CO^+ lies at 14.0136 eV.[16] The first excited ionic state $A\,^2\Pi$ has an ionization energy of 16.536 eV.[33] Since our experiments are carried out at a three-photon energy ~16.2 eV, we access an energy region only ~0.4 eV below $A\,^2\Pi$, where a plethora of superexcited states belonging to series converging upon $A\,^2\Pi$ can be expected. The energy region above the lowest ionic threshold of CO has been studied in some detail in a number of previous studies.[16,34–37] We shall focus on a VUV one-photon absorption study of Huffman *et al.*[34] and a vibrationally resolved photoionization cross section study of Leyh *et al.*[36] They show in the wavelength region 70–80 nm important Rydberg series converging upon the $A\,^2\Pi$ ionic state.

The strongest deviation of the Franck–Condon behavior, with v^+ levels populated up to 4, is observed for resonance enhancement near the electronic origin of the $B\,^1\Sigma^+$ state, where low rotational levels are accessed. The three-photon energy of 16.17 eV, at which this strong non-Franck–Condon behavior is observed, corresponds rather closely to a feature at 76.67–76.69 nm in the one-photon absorption spectrum of Fig. 4 of Ref. 34. This feature has been assigned by Leyh *et al.*[36] as composed of the $5'd'\delta$ $(v=1)$ and the $'5s+4d'\sigma$ $(v=3)$ members of a $P(3)$ Rydberg progression [note that we use the labeling as employed before in the literature, $P(3)$ does *not* indicate a $\Delta N=-1$ transition starting from $N=3$]. Non-Franck–Condon transitions are also observed, when rotational levels in the B state up to $N'=48$ are employed as stepping-stones. In a one- or two-photon absorption process rotational quantum numbers are not expected to change by much. However, when we consider a transition from a high rotational level in the ground state via the B state to a superexcited state with an $A\,^2\Pi$ core, the differences in rotational constants for the ground state ($B_0''=1.922\,629\ \mathrm{cm}^{-1}$), the B-state ($B_0'=1.948\,186\ \mathrm{cm}^{-1}$) and a typical superexcited state ($B_0^*\approx 1.58\ \mathrm{cm}^{-1}$) will involve very similar amounts of rotational energy in X and B states, but a significantly smaller amount of rotational energy in the superexcited state. For example, for a three-photon excitation from $N''=45$ to a superexcited state with $N^*=45$, the rotational energy in the ground state is $E_{\mathrm{rot}}''=3980\ \mathrm{cm}^{-1}$, while the rotational energy in the superexcited state is $E_{\mathrm{rot}}^*\approx 3270\ \mathrm{cm}^{-1}$. Upon excitation from $N''=45$ with three photons of 43 483.5 cm^{-1}, a superexcited state with $N^*=45$ is reached with an energy of 134 430.5 cm^{-1} above the ground state ($X\,^1\Sigma^+;v''=0,N''=0$). The origin of this superexcited state is then estimated to lie at 131 160.5 cm^{-1} (76.24 nm), and this closely corresponds to the peak measured at 76.31 nm in Ref. 34. This feature has been assigned by Leyh *et al.*[36] as the $3'd'\delta$ $(v=7)$ state.

Therefore, we can interpret our observed non-Franck–Condon diagonal transitions in terms of excitation and subsequent autoionization from different superexcited states, depending on the rotational level involved. The non-Franck–Condon peaks resulting from the rotationless excitation may arise from the autoionization from the $5'd'\delta$ $(v=1)/'5s+4d'\sigma$ $(v=3)$ superexcited states, which feature in the 76.67–76.69 nm region in the one-photon VUV absorption spectrum.[34] For higher rotational levels, for example $N''=45$, the $3'd'\delta$ $(v=7)$ state may be excited in a three-photon process, and thus lead to non-Franck–Condon behavior.

The question remains whether these superexcited states can be accessed in a one-photon transition from the $B\,^1\Sigma^+$ state, or in a three-photon transition from the $X\,^1\Sigma^+$ ground state. The one-photon excitation of the required superexcited states via the B state is formally forbidden, but may gain some intensity from effects of electron correlation, while the three-photon excitation from the $X\,^1\Sigma^+$ ground state can be quasi-resonant with and can borrow some intensity from the B state. The fact that vibrationally excited levels of these various superexcited $3'd'\delta$ $(v=7)$, $4'd'\delta$ $(v=3)$ and $5'd'\delta$ $(v=1)/'5s+4d'\sigma$ $(v=3)$ states can be accessed at all may arise from the rather large difference in equilibrium geometries between the $X\,^1\Sigma^+$ ($R_e=1.1283$ Å[22]) and the $B\,^1\Sigma^+$ Rydberg state ($R_e=1.1197$ Å[20]) on the one hand and the superexcited states possessing an $A\,^2\Pi$ ionic core ($R_e=1.2436$ Å[22]) on the other. Also, in a recent pulsed field ionization photoelectron (PFI-PE) study,[16] deviations in the rotationally resolved PFI-PE spectra were observed for the production of $v^+=6-9$ in CO^+ ($X\,^2\Sigma^+$). This region was accessed in one-photon excitation with narrow band synchrotron radiation at energies from 16–16.8 eV (see Figs. 1–3 in Ref. 16). These deviations were attributed to perturbations by near-resonant Rydberg levels. Summarizing, there is extensive discussion and evidence in the literature that in the region ~1 eV below the $A\,^2\Pi$ ionic limit autoionization plays a significant role. Therefore, we attribute the non-Franck–Condon behavior observed in our experiments on CO as arising from excitation to and subsequent autoionization from the $5'd'\delta$ $(v=1)$ and $'5s+4d'\sigma$ $(v=3)$ states at low rotational levels and $3'd'\delta$ $(v=7)$ and $4'd'\delta$ $(v=3)$ for higher rotational levels.

In the narrow energy region where the above superexcited states occur, they also affect the rotationally resolved photoelectron spectra. The rotational structure in the photoelectron spectra in the region where large deviations from $\Delta v=0$ propensity are observed shows striking asymmetries as exemplified in the photoelectron spectrum associated with ionization out of $Q(45)$. This spectrum is depicted in Fig. 5. Clearly, the $\Delta N=-1$ peak is missing, while the other transitions ($\Delta N=0,+1,\pm 2$) remain visible. Of course the calculated rotationally resolved photoelectron spectra, which would be symmetrical in the limit of classical rotation, do not predict these observations because they do not include the role of the superexcited states. Quantum interference between two isoenergetic ionization pathways, *viz.* direct ionization via excitation into the ionization continuum on the one hand, and excitation of a superexcited state followed by autoionization on the other, may lead to Fano-type line

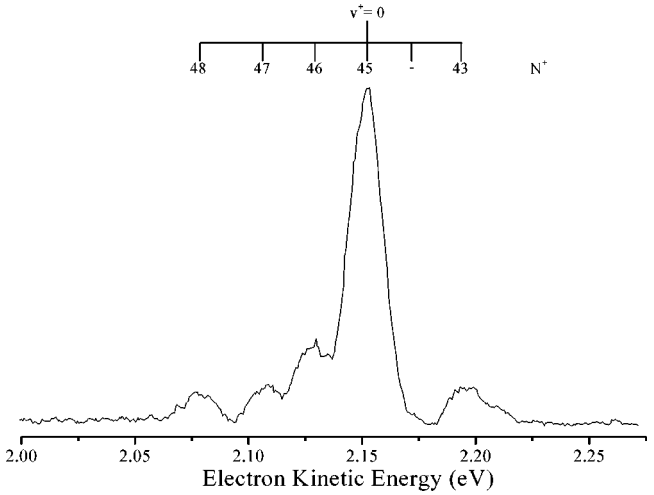

FIG. 5. Photoelectron spectra of rotationally excited CO, resulting from ionization out of the $Q(45)$ branch measured at the non-Franck–Condon energy region. The spectrum shows a missing $\Delta N=1$ peak, while the other transitions are the same as depicted in Fig. 3(a).

shapes in the excitation spectra. Associated changes in the absorption cross section may also result, as observed in our photoelectron spectra. Fano-type phenomena are a common occurrence involving superexcited states in atoms,[38,39] but have remained much more elusive so far for molecules.

V. CONCLUSIONS

Hot rotational levels of CO, photodissociated from OCS, have been studied using $(2+1)$ REMPI via the $B\,^1\Sigma^+$ Rydberg state leading to the $X\,^2\Sigma^+$ state of the ion. Improved spectroscopic rotational parameters have been obtained for the $B\,^1\Sigma^+$ state for N' up to 87. These high rotational levels show photoelectron spectra with a very strong $\Delta N=0$ transition and weaker $\Delta N=\pm 1$, ± 2, and ± 3 transitions. The agreement between measured and calculated spectra is good, indicating that there is significant angular momentum coupling in the photoelectron orbital. In the narrow energy region where the competition between direct ionization and the excitation of superexcited states is apparent, our vibrationally and rotationally resolved photoelectron spectra reveal strong non-Franck-Condon behavior and show indications for quantum interference between isoenergetic pathways.

ACKNOWLEDGMENTS

A.M.R. acknowledges the Holland Research School of Molecular Chemistry for a Ph.D. fellowship. C.A.dL. acknowledges very useful discussions with Professor J. M. Dyke and members of his group during a stay in Southampton in the context of the EC Network on Reactive Intermediates. C.A.dL. and A.M.R. acknowledge helpful discussions at the Lisbon meeting of the EC Network on Reactive Intermediates (April 2001), and thank Ing. D. Bebelaar for technical support. This work was supported by a grant from the National Science Foundation.

[1] J. W. Rabalais, J. M. McDonald, V. Scherr, and S. P. McGlynn, Chem. Rev. **71**, 73 (1971).
[2] N. Sivakumar, I. Burak, W.-Y. Cheung, P. L. Houston, and J. W. Hepburn, J. Phys. Chem. **89**, 3609 (1985).
[3] N. Sivakumar, G. E. Hall, P. L. Houston, J. W. Hepburn, and I. Burak, J. Chem. Phys. **88**, 3692 (1988).
[4] Y. Sato, Y. Matsumi, M. Kawasaki, K. Tsukiyama, and R. Bersohn, J. Phys. Chem. **99**, 16307 (1995).
[5] T. Suzuki, H. Katayanagi, S. Nanbu, and M. Aoyagi, J. Chem. Phys. **109**, 5778 (1998).
[6] Z. H. Kim, A. J. Alexander, and R. N. Zare, J. Phys. Chem. **103**, 10144 (1999).
[7] A. Sugita, M. Mashino, M. Kawasaki, Y. Matsumi, R. Bersohn, G. Trott-Kriegeskorte, and K-H. Gericke, J. Chem. Phys. **112**, 7095 (2000).
[8] R. A. Morgan, A. J. Orr-Ewing, D. Ascenzi, M. N. R. Ashfold, W. J. Buma, C. R. Scheper, and C. A. de Lange, J. Chem. Phys. **105**, 2141 (1996).
[9] R. A. Morgan, M. A. Baldwin, D. Ascenzi, A. J. Orr-Ewing, M. N. R. Ashfold, W. J. Buma, J. B. Milan, C. R. Scheper, and C. A. de Lange, Int. J. Mass Spectrom. Ion Processes **159**, 1 (1996).
[10] A. M. Rijs, E. H. G. Backus, C. A. de Lange, N. P. C. Westwood, and M. H. M. Janssen, J. Electron Spectrosc. Relat. Phenom. **112**, 151 (2000).
[11] E. de Beer, C. A. de Lange, J. A. Stephens, Kwanghsi Wang, and V. McKoy, J. Chem. Phys. **95**, 714 (1991).
[12] E. de Beer, M. Born, C. A. de Lange, and N. P. C. Westwood, Chem. Phys. Lett. **186**, 40 (1991).
[13] Kwanghsi Wang, J. A. Stephens, V. McKoy, E. de Beer, C. A. de Lange, and N. P. C. Westwood, J. Chem. Phys. **97**, 211 (1992).
[14] J. B. Milan, W. J. Buma, C. A. de Lange, Kwanghsi Wang, and V. McKoy, J. Chem. Phys. **107**, 2782 (1997).
[15] C. A. de Lange, in *The Role of Rydberg States in Spectroscopy and Reactivity*, edited by C. Sandorfy (Kluwer Academic, New York, 1999), p. 457.
[16] M. Evans and C. Y. Ng, J. Chem. Phys. **111**, 8879 (1999).
[17] A. M. Rijs, E. H. G. Backus, C. A. de Lange, M. H. M. Janssen, Kwanghsi Wang, and V. McKoy, J. Chem. Phys. **114**, 9413 (2001).
[18] R. R. Lucchese, G. Raseev, and V. McKoy, Phys. Rev. A **25**, 2572 (1982).
[19] Kwanghsi Wang and V. McKoy, J. Chem. Phys. **95**, 4977 (1991).
[20] M. Eidelsberg, J.-Y. Roncin, A. Le Floch, F. Launay, C. Letzelter, and J. Rostas, J. Mol. Spectrosc. **121**, 309 (1987).
[21] G. Sha, D. Proch, Ch. Rose, and K. L. Kompa, J. Chem. Phys. **99**, 4334 (1993).
[22] K. P. Huber and G. Herzberg, *Molecular Spectra and Molecular Structure*, Vol. 4, *Constants of Diatomic Molecules* (Van Nostrand Reinhold, New York, 1978).
[23] S. G. Tilford and J. T. Vanderslice, J. Mol. Spectrosc. **26**, 419 (1968).
[24] C. E. Moore, *Atomic Energy Levels*, NBS Circ. 467, Vol. 1, Natl. Bur. Std., Washington, 1949.
[25] W. C. Martin, R. Zalubas, and A. Musgrave, J. Phys. Chem. Ref. Data **19**, 821 (1990).
[26] W. J. Hunt and W. A. Goddard, Chem. Phys. Lett. **3**, 414 (1969).
[27] W. Kong, D. Rodgers, J. W. Hepburn, Kwanghsi Wang, and V. McKoy, J. Chem. Phys. **99**, 3159 (1993).
[28] G. Guelachvili, D. de Villeneuve, R. Farrenq, W. Urban, and J. Verges, J. Mol. Spectrosc. **98**, 64 (1983).
[29] J. Xie and R. N. Zare, J. Chem. Phys. **93**, 3033 (1990).
[30] S. N. Dixit and V. McKoy, Chem. Phys. Lett. **128**, 49 (1986).
[31] C. A. de Lange, J. Chem. Soc. Faraday Trans. **94**, 3409 (1998).
[32] C. A. de Lange, Adv. Chem. Phys. **117**, 1 (2001).
[33] Y. Tanaka, Sci. Pap. Inst. Phys. Chem. Res. (Jpn.) **39**, 447 (1942).
[34] R. E. Huffman, J. C. Larrabee, and Y. Tanaka, J. Chem. Phys. **40**, 2261 (1964).
[35] M. Ogawa and S. Ogawa, J. Mol. Spectrosc. **98**, 393 (1972).
[36] B. Leyh, J. Delwiche, M.-J. Hubin-Franskin, and I. Nenner, Chem. Phys. **115**, 243 (1987).
[37] J. E. Hardis, T. A. Ferrett, S. H. Southworth, A. C. Parr, P. Roy, J. L. Dehmer, P. M. Dehmer, and W. A. Chupka, J. Chem. Phys. **89**, 812 (1988).
[38] P. van der Meulen, M. O. Krause, and C. A. de Lange, Phys. Rev. A **43**, 5997 (1991).
[39] P. van der Meulen, M. O. Krause, C. D. Caldwell, S. B. Whitfield, and C. A. de Lange, Phys. Rev. A **46**, 2468 (1992).